

An anomalous band inversion protected by symmetry in a topological insulator of the Kane-Mele model

Jie-Xiang Yu and J. G. Che*

Surface Physics Laboratory (National Key Laboratory),

Key Laboratory of Computational Physical Sciences (MOE),

Department of Physics and Collaborative Innovation Center of Advanced Microstructures,

Fudan University, Shanghai 200433, People's Republic of China

Abstract

Depositing Au on a graphene derivative, which involves substituting four C atoms with three N atoms in a 3×3 cell graphene, we realized a topological insulator of the Kane-Mele model with a gap of 50 meV surrounding the Dirac point of graphene. In this material, we observed an anomalous band inversion (BI) protected by the symmetry with character e of group C_{3v} . The symmetry constrains two e bands with mirror-symmetry combination (MSC) and mirror-antisymmetry combination (MAC) of Au and N orbitals degenerate at Γ , whereas the interaction of π^* of graphene on the e -MAC band tends to lift this degenerate, resulting in that the π^* and e -MAC band exchange their orbital components near Γ , causing thus a discontinued BI.

PACS numbers: 73.43.-f, 71.70.Ej, 71.15.Mb, 73.22.Pr

Kane and Mele suggested in their primary work that a two-dimensional (2D) topological insulator (TI) could be realized in graphene.[1] The 2D TI is called a Quantum spin Hall (QSH) insulator.[1] However, it is difficult to experimentally observe its topological gap because of graphene's very weak spin-orbit coupling (SOC).[2–5] Due to its potential applications, Kane and Mele's suggestion has promoted significant research efforts to realize 2D TI in graphene.[6–9] Young *et al.* [9] confirmed that the QSH state could be experimentally observed in a charge-neutral graphene under a very large magnetic field. A graphene having certain heavy adatoms was predicted by Week *et al.* [7] to realize a TI with substantial band gap. A similar method to obtain a gap exceeding 0.2 eV without tuning the Fermi level to enter the TI state was suggested by Hu *et al.* [8] It was reported that the graphene related heterostructure (graphene sandwiched between two strong SOC materials such as Bi₂Se₃) could enhance the intrinsic SOC of graphene and open a topological non-trivial gap.[10–12] As a material for use in next-generation electronic devices, graphene is stable and shows remarkable properties. Realizing a graphene-templated TI in combination with advanced technology have a wide array of applications, from spintronics to quantum information process.[13, 14]

In the present work, we propose a platform based on a graphene derivative to realize a topological insulator of the Kane-Mele model. The graphene template involves substituting four C atoms with three N atoms in a 3×3 graphene cell ($g\text{-C}_{14}\text{N}_3$). After Au is deposited on $g\text{-C}_{14}\text{N}_3$, two bands of the interaction between Au and N are characterized by irreducible representation e of group C_{3v} . The symmetry constrains the two e bands with mirror-symmetry combination (MSC) and mirror-antisymmetry combination (MAC) of Au and N orbitals degenerate at Γ , whereas the interaction of π^* on the e -MAC band tends to lift this degenerate, resulting in that a piece of the e -MAC band near Γ exchanges with a piece of the π^* band, causing thus a discontinued BI between the π^* and e -MAC band. This anomalous BI protected by symmetry leads to a topological nontrivial gap of 50 meV around the Dirac point of graphene.

The results were obtained by our first-principles calculations on the framework of density functional theory with the projector augmented plane-wave (PAW) potential [15] as implemented in VASP package[16]. The exchange-correlation energy was described by local density approximation (LDA),[17] which treated the atomic positions well in the graphene-based structures.[18] The wave functions were expanded in a plane-wave with an energy

cutoff of 600 eV throughout calculations. The k points in surface Brillouin zone (BZ) of the 3×3 unit cell of graphene-based structures were sampled on a Γ -centered 7×7 mesh. All atoms could be relaxed until the Hellmann-Feynman forces on the atoms were less than 0.001 eV/Å. We performed the maximally localized Wannier function (MLWF) process implemented in Wannier90 package for fitting tight-binding Hamiltonian and analyzing the evolution of the Wannier function center (WFC).[21]

Lee *et al.* synthesized a graphitic carbon nitride material, which can be seen as four C atoms are substituted by three N atoms in a 2×2 unit cell of graphene, $g\text{-C}_4\text{N}_3$.[22] However, by observing its electronic structures, we found that this material was not suitable for inverting the bands around the Fermi level because of its large 2 eV gap.[23] This large gap was caused by the substitution of four C atoms with three N atoms, which completely breaks π -bonds in a 2×2 graphene cell that is critical for forming the Dirac cone. Since the large gap can be seen because very few $C(pz)$ pairs existed in $g\text{-C}_4\text{N}_3$, extending its reassembly is worthwhile. To realize 2D TI based on graphene with the Dirac-like point near the Fermi level, as suggested by Kane and Mele,[1] a simple and effective approach is to extend the graphene unit cell from 2×2 to 3×3 size ($g\text{-}3 \times 3$), as shown in Fig. 1, hereafter referred to as $g\text{-C}_{14}\text{N}_3$. $g\text{-C}_{14}\text{N}_3$ can be seen as a patterned graphene. As Kim *et al.* suggested, nanoscale patterns can be made in a horizontally prepatterned graphene using standard lithography techniques.[25] In that case, the Kane-Mele's model TI may be realized by depositing strong SOC elements such as Au on $g\text{-C}_{14}\text{N}_3$. The Dirac point appears again because more π -bonds existed in $g\text{-C}_{14}\text{N}_3$ than in $g\text{-C}_4\text{N}_3$. We can see below that the +1e hole with the Dirac point 0.1 eV above the Fermi level in $g\text{-C}_{14}\text{N}_3$ plays an important role in forming TI after Au is adsorbed on $g\text{-C}_{14}\text{N}_3$. Considering the stability of $g\text{-C}_4\text{N}_3$ obtained by Du *et al.*, [23] $g\text{-C}_{14}\text{N}_3$ can be also expected to be stable.

It is well known that a stable crystal with vacancies should be those with the least broken bonds.[24] We accordingly considered the stability of $g\text{-C}_{14}\text{N}_3$. Following this criterion, only three possible configurations by removing four C atoms at sites a-b-c-d (chair), a-b-c-e (boat) and b-c-d-e (star type) in Figure 1 need to be taken into account. The criterion also dominates the most stable configuration for depositing three N atoms on the graphene with vacancies. That is, in order to reduce the number of broken bonds, all three N atoms favor to occupy the vacancy sites. Due to the symmetry, there are two inequivalent configurations for three N atoms on four vacancies of the boat and chair type. We optimized the five con-

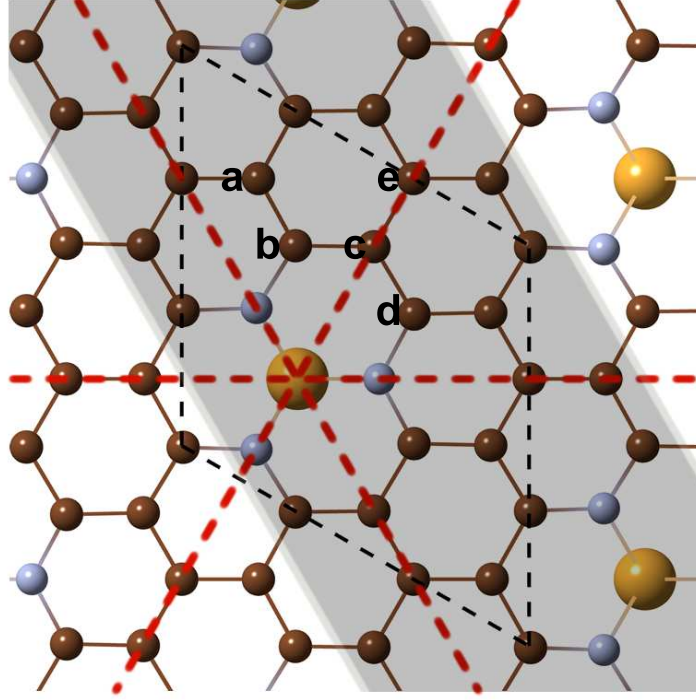


FIG. 1: (Color online) Topview of the atomic configuration for $g\text{-C}_{14}\text{N}_3$. Brown, blue and yellow balls represent C, N and Au, respectively. Thin-dashed lines denote the boundary of a 3×3 unit cell of graphene with three mirror-symmetric planes, which are identified by three red thick-dashed lines. The shadow region indicates the structure of a 1D ribbon with an armchair edge. Labels a, b, c, d and e indicate different vacancy-chainis, see text.

figurations. The total energy of the optimized configuration of N on the star-type vacancies ($g\text{-C}_{14}\text{N}_3$) is at least 2 eV lower than that of N on the boat- and chair-type vacancies.

Owing to its importance, we first focus on the electronic structure of $g\text{-C}_{14}\text{N}_3$. As mentioned above, $g\text{-C}_{14}\text{N}_3$ can be seen a derivative of a 3×3 unit cell of graphene ($g\text{-}3 \times 3$), in which four C atoms are substituted by three N atoms. N replaces the position of C with only a relatively small displacement: the length of the N-C bond is 1.34 Å, whereas that of the C-C bond in graphene 1.42 Å.[26, 27] The displacement of N in the direction perpendicular to the graphene plane is 0.08×10^{-4} Å, smaller than our calculated accuracy. In other words, three N atoms lie in the same plane as that of C.

We plotted the band structures of $g\text{-C}_{14}\text{N}_3$ in Fig. 2 (a). The band structures of the graphene in the 3×3 size unit cell ($g\text{-}3 \times 3$) are also given in Fig. 2 (b) for comparison. Compared with the band structures of the graphene in the 1×1 unit cell ($g\text{-}1 \times 1$), two

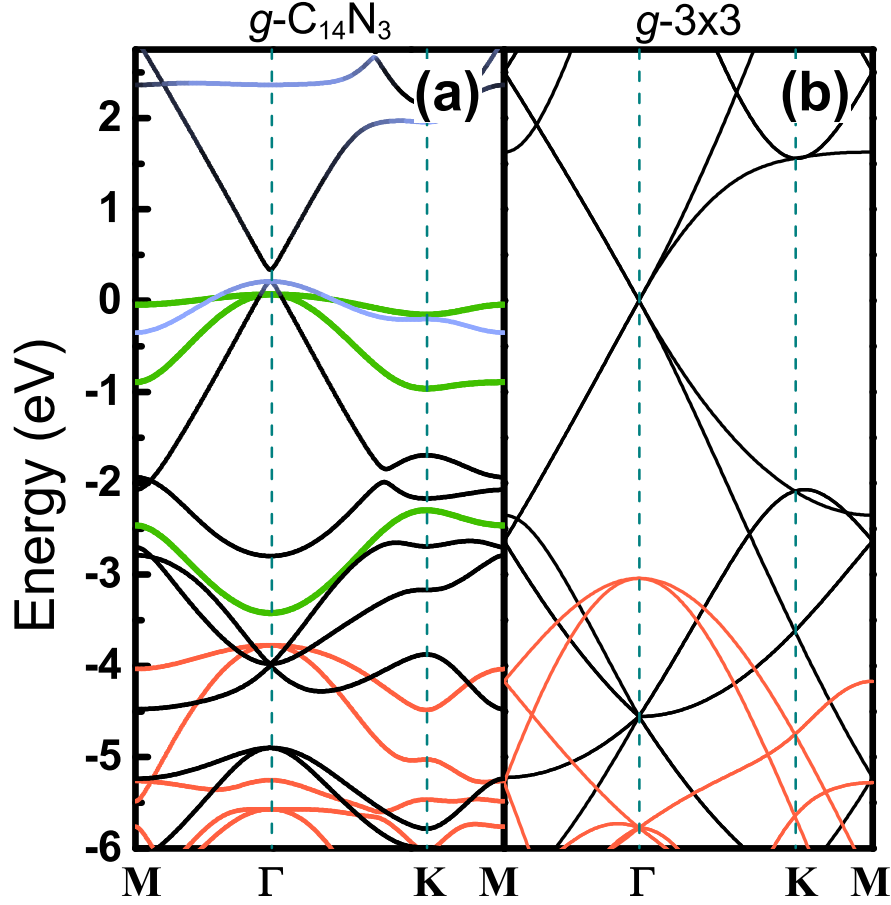


FIG. 2: (Color online) Band structure of $g\text{-C}_{14}\text{N}_3$ (a) and $g3 \times 3$ (b). Green lines denote the bands consisting of N's lone pairs, blue lines denote the bands consisting of about 25% $\text{N}(p_z)$ and 27% $\text{C}(p_z)$ orbitals, and red lines denote σ bonds of C-C with sp^2 hybridization.

features for $g-3 \times 3$ should be addressed: (1) The Dirac point of $g-1 \times 1$ is folded from the K point of $g-1 \times 1$ to the Γ point of $g-3 \times 3$; and (2) along the Γ -M axis, the bands surrounding the Fermi level are twofold degenerate, whereas along the Γ -K axis, this degenerate is lifted. This can be expected, since the axis along Γ -K in the BZ of $g-3 \times 3$ has two unequivalent ways to fold from the axes along K- Γ and K-M in the BZ of $g-1 \times 1$. Below, we name them π - and π' -bonding states, respectively, whereas π^* and π'^* are their antibonding states.

Although four C atoms are replaced by three N atoms in $g-3 \times 3$, the π and π^* band are almost unaffected by N in $g\text{-C}_{14}\text{N}_3$ compared with those in $g-3 \times 3$. However, a 0.1 eV gap is opened around the Dirac point and, the Fermi level shifts down by 0.2 eV with respect to the top of the occupied π band, leaving a $+1e$ hole. The $+1e$ hole can be expected since four

C atoms with 16 valence electrons are substituted by three N atoms with only 15 valence electrons.

In contrast, the π' and π'^* band in g - 3×3 disappear in g - $C_{14}N_3$. Instead, there is a bonding band near the Fermi level, consisting of about 25% $N(p_z)$ and 75% $C(p_z)$ orbitals, which also degenerate with π at the Γ point, and an antibonding band 2.5 eV above the Fermi level. Both the bonding and antibonding band are shown by blue lines in Fig. 2 (a). They are still referred to as π' and π'^* in the following discussion. The separation in energy between the π' and π'^* band is about 2.5 eV, consistent with the gap in g - C_4N_3 , [23] which can also be seen as a graphene derivative with the same substitution formula. In g - C_4N_3 , the Dirac point disappeared. [23] However, in g - $C_{14}N_3$, a 0.1 eV gap is opened around the Dirac point.

The band difference between g - $C_{14}N_3$ and g - 3×3 is observed mainly in the energy region between -4 and 2 eV, as shown in the figure by the blue and green lines. Three green bands can be attributed to the interaction between three dangling bonds of N's sp^2 hybridization, the so-called lone pairs. The three dangling bonds of N interact with each other and form one singlet a_1 and two doublet e states characterized by group C_{3v} . At the Γ point, a_1 and e lie at -3.5 eV and near the Fermi level, respectively. The e bands arising from the orbital mirror-symmetric combination (MSC) and mirror-antisymmetric combination (MAC) of N's sp^2 hybrids are degenerate at the Γ point and disperse away from it, with the MSC band always below the MAC band, as shown in the figure. The topological nontrivial gap of graphene calculated by us is less than 10^{-3} meV, in agreement with the earlier calculation. [4] However, from the aspect of experiment, the gap is too small to be observed. [2–5] We will focus on the SOC effect in terms of introducing elements such as Au with strong SOC. We will see below that the evolution of these bands upon interaction with deposited Au shows that g - $C_{14}N_3$ is a good platform for realizing the Kane-Mele's TI.

Among all inequivalent adsorption (six top, six bridge and three hollow) sites considered for Au adsorption on g - $C_{14}N_3$, the most stable one, at least 0.8 eV lower than the others, is shown in Fig. 1: Au is lifted by 1.68 \AA away from the graphene layer, and the upward shift of three N atoms to the graphene layer is less than 0.07 \AA . Each N is bonded to two neighbor C atoms with a length of C-N of 1.36 \AA . The C-N-C angle is 123° , which is a slightly larger than that of C atoms in graphene (120°). The adsorption of Au on g - $C_{14}N_3$ gains an energy of 2.6 eV.

In order to further confirm the stability of $\text{Au}/g\text{-C}_{14}\text{N}_3$, we performed a phonon calculation implemented in VASP package.[16] In the calculation, the density functional perturbation theory [28] was used to calculate force constants, of which the concerned derivatives were determined by linear response with respect to changes in the ionic positions. There are no imaginary frequencies associated with distortion of $\text{Au}/g\text{-C}_{14}\text{N}_3$, indicating its stability.

Band structures of $\text{Au}/g\text{-C}_{14}\text{N}_3$ with and without SOC were calculated and are shown in Fig. 3 (a) and (b), respectively. Fig. 3 (c) is an enlargement of the dashed-rectangle portion in Fig. 3 (b). The band structures with SOC (Fig. 3(a)) show a gap of 50 meV surrounding the Dirac point.

Here the key is that the electronic properties of $g\text{-C}_{14}\text{N}_3$ showed a $+1e$ hole with the Dirac point 0.1 eV above the Fermi level. After adsorption of Au in a $d^{10}s^1$ configuration on $g\text{-C}_{14}\text{N}_3$, the Fermi level returns to the Dirac point. Simultaneously, the s and d_{xz}/d_{yz} orbitals of Au have to form an sd^2 hybridization to adapt to the $g\text{-C}_{14}\text{N}_3$ with the threefold coordination of N. Thus, d -electrons of Au with strong SOC appear around the Fermi level, resulting in the topological nontrivial gap.[29, 30]

The topological nontrivial properties of $\text{Au}/g\text{-C}_{14}\text{N}_3$ can be verified by the evolution of the Wannier function center (WFC) and the band structures of a 2D stack ribbon of $\text{Au}/g\text{-C}_{14}\text{N}_3$, as shown in Fig. 4 (a) and (b), respectively. The WFC in reciprocal space during a "time-reversal pumping" process was calculated by the $U(2N)$ non-Abelian Berry connection.[21] $\text{Au}/g\text{-C}_{14}\text{N}_3$ can be seen as a 1D ribbon with an armchair edge periodically stacking along the direction perpendicular to the edge of the 1D-ribbon, whose unit cell has two Au, six N and 28 C atoms as shown by the shadow region in Fig. 1. The band structures shown in Fig. 4 (b) were obtained by calculating a stack ribbon with 50 1D ribbons of $\text{Au}/g\text{-C}_{14}\text{N}_3$, whose interaction parameters were obtained by the MLWF method.[20, 31] We confirmed that the stack ribbon with 50 1D-ribbons is wide enough to avoid the interaction between the two edges over the stack ribbon. The odd winding number of the WFC and the gapless edge states of the stack ribbon, shown in Fig. 4 (a) and (b), respectively, confirm [21] that a topological nontrivial phase appears after Au is deposited on $g\text{-C}_{14}\text{N}_3$.

Next, we focus on the bands near the Fermi level without SOC (Fig. 3 (b)). With the help of the orbital information (green: Au+N orbitals $> 74\%$, red: π^* orbitals $> 74\%$), the bands near the Fermi level of $\text{Au}/g\text{-C}_{14}\text{N}_3$ can be understood. At first glance, both the dispersion and orbitals of two bands, which are distributed in the energy region between

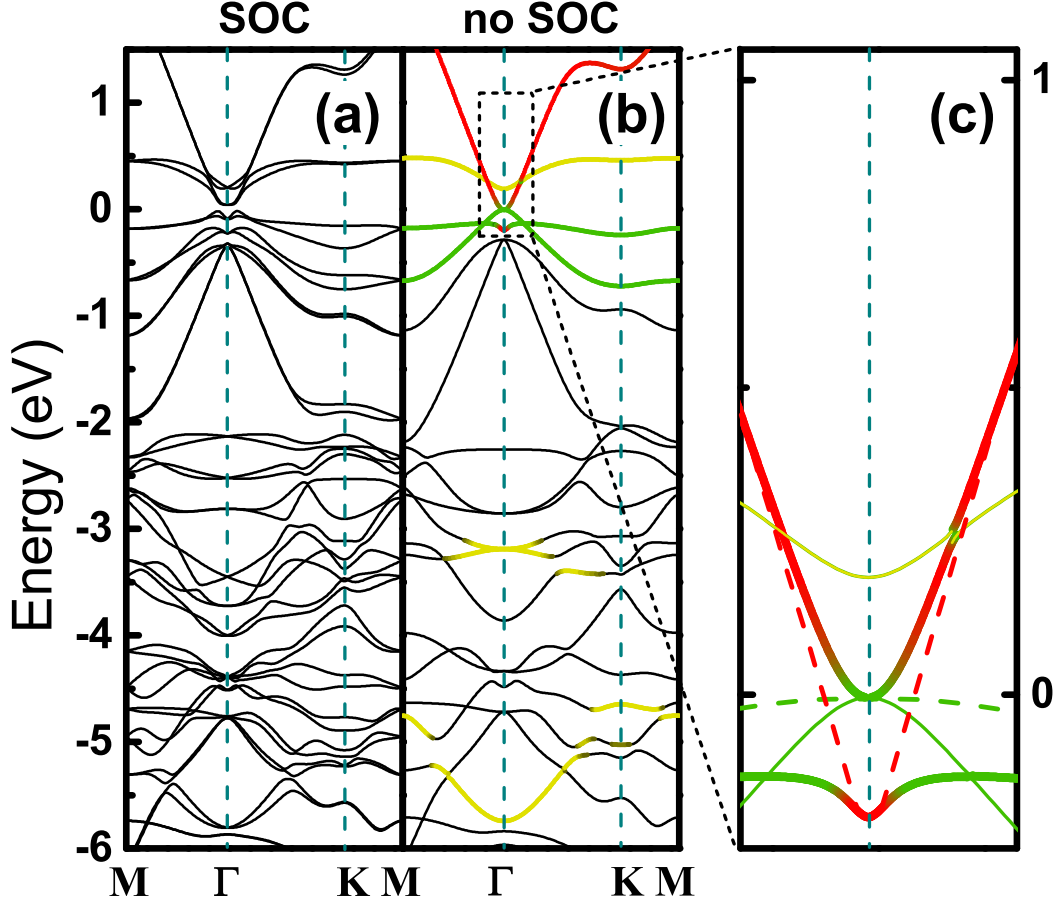


FIG. 3: (Color online) Band structure of Au/*g*-C₁₄N₃ (a) with and (b) without SOC. The green and yellow lines denote the bands primarily consisting of Au and N orbitals, and the red lines denote the π^* band. Panel (c) is an enlargement of the dashed-rectangle portion in panel (b) in order to more clearly illustrate the discontinued thick green and red bands. A conventional band inversion is schematically described by the dashed green and red lines in panel (c).

-0.2 and -2.2 eV and degenerated at the Γ point, are similar to that of the π and π' bands of *g*-C₁₄N₃. That is, the two bands are less affected by the adsorption of Au compared with that in *g*-C₁₄N₃. However, owing to the Au deposition, the Fermi level is now found to be at the bottom of the π^* band, indicating that the two bands are now fully filled and that the top of both bands, which degenerate at Γ , lies -0.2 eV below the Fermi level. This implies that the $+1e$ hole has been fully filled. The topmost occupied bands are now the bands with the e symmetry of C_{3v}, indicated by thick and thin green lines. Thus, in comparison with the band order in *g*-C₁₄N₃, a BI between the π (π') and the e bands occurs because of Au

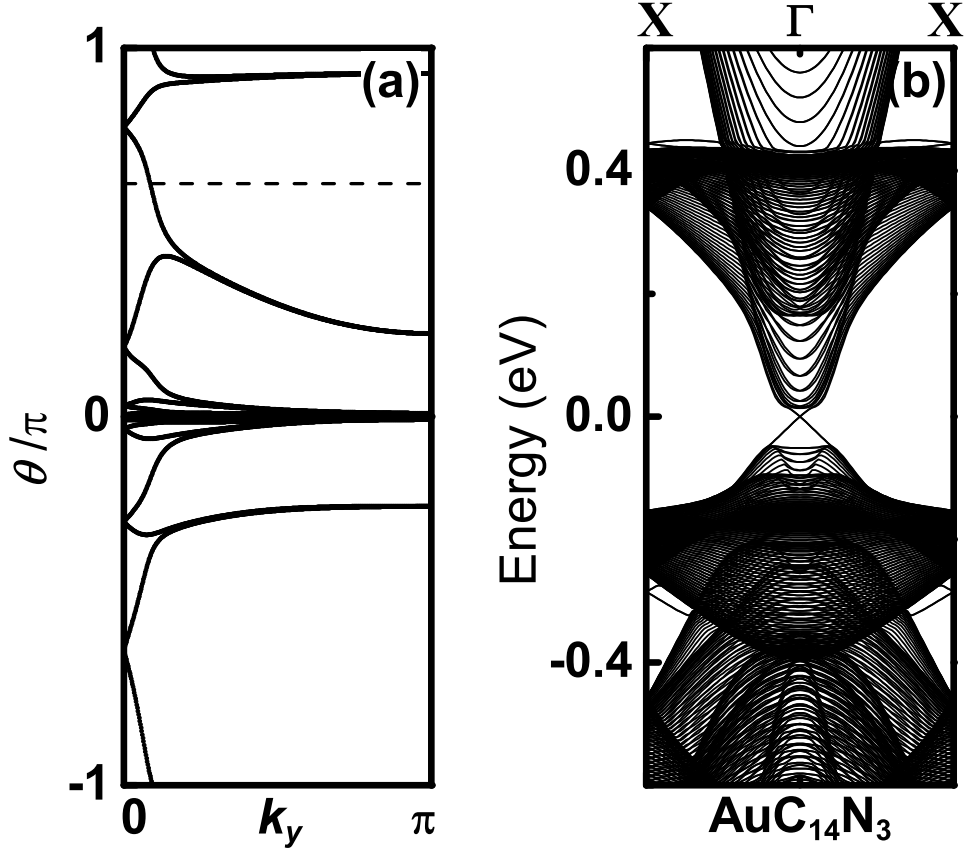


FIG. 4: Evolution of the Wannier function center (a) and band structures of the stack ribbon of Au/g-C₁₄N₃ (b). The dashed line in panel (a) is used as a reference.

adsorption.

Furthermore, the a_1 and e bands arising from the interaction of three N's lone pairs in the g -C₁₄N₃, as shown by the green lines ranging from 0.0 to -3.5 eV in Fig. 2 (a), have disappeared. Instead, two green and three yellow bands exist below the Fermi level; these five bands can be traced to the interactions between Au and N, implying that Au has broken the lone pair bonds of the three N atoms.

In order to adapt to the threefold coordination of the N atoms, the s and d_{xz}/d_{yx} orbitals of Au have to form an sd^2 hybridization. Therefore, the two interaction bands between Au and N, the thick and thin green bands near the Fermi level in Fig. 3 (c), keep the same e symmetry as the lone pair bands of N in g -C₁₄N₃, i.e., the bands with MSC and MAC of Au and N orbitals, corresponding to the e irreducible representation of C_{3v}. [32].

The orbital analysis of the e band (thick green) and π^* band (thick red) band, as shown in Fig. 3 (b) and (c), identifies from their color that their orbital components are exchanged

at 0.0 eV and -0.2 eV, respectively. This means that without SOC the two bands (thick green and red) are inverted near the Γ point. In contrast to a conventional BI, however, both inverted bands are *discontinuous* in the orbital components (indicated by color). Considering the e symmetry for the thick (MAC) and thin green (MSC) bands, and the a_2 symmetry for the thick red (MAC) band, the anomalous BI can be understood.

In $g\text{-C}_{14}\text{N}_3$, the e bands consist of MSC and MAC of N's orbitals. In the entire BZ, the e band with MSC is lower in energy than that with MAC, as shown in Fig. 2 (a). After Au adsorption, the bonds between the three N's lone pairs are broken, forming the interaction bonds between Au and N consisting of the s and d_{xz}/d_{yz} orbitals of Au (sd^2 hybrids) and the s and p_x/p_y orbitals of N (sp^2 hybrids). Hereafter, the two bands are referred to as Au+N. Most importantly, the Au+N bands have the same e symmetry (MSC and MAC) as the bands of the three N's lone pairs in $g\text{-C}_{14}\text{N}_3$, as discussed above. Therefore, if there are no perturbations of π^* , the dispersion of the e band with MAC should be schematically described by the dashed green line in Fig. 3 (c), i.e., the dashed green line and the thin green line are degenerate at the Γ point and disperse away from it, similar to that in $g\text{-C}_{14}\text{N}_3$, as shown by the two green lines near the Fermi level in Fig. 2 (a).

As we have seen from the band structures of $g\text{-C}_{14}\text{N}_3$ in Fig. 2 (a), the e band with MSC is lower in energy than those with MAC along the axis M- Γ -K. In contrast, for Au/ $g\text{-C}_{14}\text{N}_3$, approaching the Γ point the e band with MAC (thick green line) first crosses over and then is lower than the e band with MSC (thin green line), as shown in Fig. 3 (c). We now try to understand the physics behind the observation.

Since Au does not lie in the same plane as N and C (1.68 Å above), the thick and thin green bands are mixed with a few p_z orbitals of both N and C, indicating the interaction between Au+N and π^* . Thus, the dispersion of the Au+N band with MAC is affected. The dashed green band in Fig. 3 (c) can be viewed as an unaffected e band with MAC, keeping its energy order relative to the thin green line (the e band with MSC), similar to the two e bands in $g\text{-C}_{14}\text{N}_3$ shown in Fig. 2 (a). Due to the interaction with π^* , the thick green band is lower in energy than the dashed green band. This can be seen as the first interaction on the e band with MAC (thick green line). In fact, there is also an interaction between π^* and the e band with MSC (thin green line). However, since π^* consists of the orbitals of MAC, the interaction between the bands with MSC and MAC cancelled out each other.

It is well known that for the bands with e symmetry of C_{3v} , its MSC and MAC states

are constrained to degenerate at the Γ point.[32] This symmetry constraint can be seen as the second interaction with an opposite direction to the first one. This symmetry constraint reaches its maximum at the Γ point and weakens away from it.

Thus, we can understand that the anomalous BI is a result of the competition between the first and second interaction mentioned above. On approaching the Γ point, due to this competition a piece of the thick green band with MAC (Au+N) switches from the band at -0.2 eV to the band at 0.0 eV, being degenerate with the thin green band with MSC because of the symmetric constraint, and a piece of the thick red band with MSC (π^*) does the opposite in order to retain the band continuity at -0.2 eV, as shown in Fig. 3 (c). That is, the constraint of symmetry and band continuity makes an exchange of the orbital components between the thick green and red band near the Γ point, leading to a BI. In contrast to a conventional BI, both the thick green and red band are discontinuous, and the discontinued BI is protected by symmetry. To the best of our knowledge, this anomalous BI has not been reported before.

The intrinsic SOC of the graphene sandwiched between Bi_2S_3 layers with strong SOC could be enhanced, leading to a BI between the conducting band of Bi_2S_3 and the valence band of graphene.[10] The mechanism of the graphene related heterostructures is similar.[11, 12] In contrast, the BI of Au/ $g\text{-C}_{14}\text{N}_3$ is driven by the band exchange constrained by the symmetry, as mentioned above.

In summary, by showing the existence of a topological nontrivial gap of 50 meV surrounding the Dirac point of graphene, we demonstrate through first-principles calculations that a Kane-Mele TI [1] could be realized by depositing Au on $g\text{-C}_{14}\text{N}_3$, which involves substituting four C atoms with three N atoms in a 3×3 unit cell of graphene. The key to understand the TI phase lies in understanding the electronic structures of $g\text{-C}_{14}\text{N}_3$, wherein there exists a Dirac point with a $+1e$ hole. Its electronic properties play an important role as follows: (1) Following deposition of Au with 11 valence electrons on $g\text{-C}_{14}\text{N}_3$, the $+1e$ hole is filled and the Fermi level returns to the Dirac point. (2) To adapt to the threefold coordination of three N atoms in $g\text{-C}_{14}\text{N}_3$, the s and d_{xz}/d_{yz} orbitals of Au hybridize, causing the d electrons with strong SOC to appear at the Fermi level. (3) An anomalous BI between the π^* band and the Au+N band with MAC is formed, leading to a topological nontrivial gap of 50 meV surrounding the Dirac point. We note that the occurrence of a conventional BI depends on a profile of the interaction between the two involved bands, however, this anomalous BI is

protected by symmetry, independent of the interaction between the two involved bands.

This work was supported by NFSC (No.61274097) and NBRPC (No. 2011CB921803 and 2015CB921401).

* Corresponding author. E-mail: jgche@fudan.edu.cn.

- [1] C. L. Kane, and E. J. Mele, Phys. Rev. Lett. **95**, 226801 (2005).
- [2] D. Huertas-Hernando, F. Guinea, and A. Brataas, Phys. Rev. B **74**, 155426 (2006).
- [3] H. Min, J. E. Hill, N. A. Sinitsyn, B. R. Sahu, L. Kleinman, and A. H. MacDonald, Phys. Rev. B **74**, 165310 (2006).
- [4] Y. Yao, F. Ye, X.-L. Qi, S.-C. Zhang, and Z. Fang, Phys. Rev. B **75**, 041401 (2007).
- [5] M. Gmitra, S. Konschuh, C. Ertler, C. Ambrosch-Draxl, and J. Fabian, Phys. Rev. B **80**, 235431 (2009).
- [6] J. E. Moor, Nature **464**, 194 (2010).
- [7] C. Weeks, J. Hu, J. Alicea, M. Franz, and R. Wu, Phys. Rev. X **1**, 021001 (2011).
- [8] J. Hu, J. Alicea, R. Wu, and M. Franz, Phys. Rev. Lett. **109**, 266801 (2012).
- [9] A. F. Young, J. D. Sanchez-Yamagishi, B. Hunt, S. H. Choi, K. Watanabe, T. Taniguchi, R. C. Ashoori, and P. Jarillo-Herrero, Nature **505**, 528 (2014).
- [10] L. Kou, B. Yan, F. Hu, S.-C. Wu, T. O. Wehling, C. Felser, C. Chen, and T. Frauenheim, Nano Lett. **13**, 6251 (2013).
- [11] L. Kou, S.-C. Wu, C. Felser, T. Frauenheim, C. Chen, and B. Yan, ACS Nano **8**, 10448 (2014).
- [12] L. Kou, F. Hu, B. Yan, T. Frauenheim, and C. Chen, Nanoscale **6**, 7474 (2014).
- [13] A. K. Geim, and K. S. Novoselov, Nat. Mater. **6**, 183 (2007).
- [14] M. Xu, T. Liang, M. Shi, and H. Chen, Chem. Rev. **113**, 3766 (2013).
- [15] P. E. Blöchl, Phys. Rev. B **50**, 17953 (1994).
- [16] G. Kresse and J. Furthmüller, Comput. Mater. Sci. **6**, 15 (1996); Phys. Rev. B **54**, 11169 (1996); G. Kresse and D. Joubert, Phys. Rev. B **59**, 1758 (1999).
- [17] J. P. Perdew and A. Zunger, Phys. Rev. B **23**, 5048 (1981).
- [18] Q. J. Wang and J. G. Che, Phys. Rev. Lett. **103**, 066802 (2009).
- [19] A. A. Mostofi, J. R. Yates, Y.-S. Lee, I. Souza, D. Vanderbilt, and N. Marzari, Comput. Phys. Commun. **178**, 685 (2008).

- [20] N. Marzari, A. A. Mostofi, J. R. Yates, I. Souza, and D. Vanderbilt, *Rev. Mod. Phys.* **84**, 1419 (2012).
- [21] A. A. Soluyanov and D. Vanderbilt, *Phys. Rev. B* **83**, 235401 (2011); R. Yu, X. L. Qi, A. Bernevig, Z. Fang, and X. Dai, *Phys. Rev. B* **84**, 075119 (2011).
- [22] J. S. Lee, X. Wang, H. Luo, and S. Dai, *Adv. Mater.* **22**, 1004 (2010).
- [23] A. Du, S. Sanvito, and S. C. Smith, *Phys. Rev. Lett.* **108**, 197207 (2012).
- [24] J. Dabrowski and H. J. Mussig, *Silicon Surfaces and Formation of Interfaces*. World Scientific Publishing Co. Pte. Ltd: Singapore, Singapore, **2000**.
- [25] K. S. Kim, Y. Zhao, H. Jang, S. Y. Lee, J. M. Kim, K. S. Kim, J.-H. Ahn, P. Kim, J.-Y. Choi, and B. H. Hong, *Nature* **457**, 706 (2009).
- [26] P. R. Wallace, *Phys. Rev.* **71**, 622 (1947).
- [27] J. C. Slonczewski, and P. R. Weiss, *Phys. Rev.* **109**, 272 (1958).
- [28] Hui Wang and J. G. Che, *EuroPhys Lett.* **96**, 67012 (2011).
- [29] G. Bian, L. Zhang, Y. Liu, T. Miller, and T. C. Chiang, *Phys. Rev. Lett.* **108**, 186403 (2012).
- [30] G. Bian, T. Miller, and T. C. Chiang, *J. Electron Spectros. Relat. Phenom.* **201**, 36 (2015).
- [31] Z. Wei, Y. Rui, Z. Hai-Jun, D. Xi, and F. Zhong, *New J. Phys.* **12**, 065013 (2010).
- [32] S. Sugano Y. Tanabe H. Kamimura, *Multiplets of Transition-Metal Ions in Crystals* (Academic Press, New York and London, 1970).
- [33] X. Qian, J. Liu, L. Fu, and J. Li, *Science* **346**, 1344 (2014).
- [34] M. Z. Hasan, and C. L. Kane, *Rev. Mod. Phys.* **82**, 3045 (2010).
- [35] X.-L. Qi, and S.-C. Zhang, *Rev. Mod. Phys.* **83**, 1057 (2011).